Research Article

Urooj Shakir*, Aamir Ali, Muhammad Raiees Amjad, and Muyyassar Hussain

Improved gas sand facies classification and enhanced reservoir description based on calibrated rock physics modelling: A case study

https://doi.org/10.1515/geo-2020-0311
received May 08, 2021; accepted October 24, 2021

Abstract: Rock physics provides a dynamic tool for quantitative analysis by developing the basic relationship between fluid, lithological, and depositional environment of the reservoir. The elastic attributes such as impedance, density, velocity, V_p/V_s ratio, Mu-rho, and Lambda-rho are crucial parameters to characterize reservoir and non-reservoir facies. Rock physics modelling assists like a bridge to link the elastic properties to petrophysical properties such as porosity, facies distribution, fluid saturation, and clay/shale volume. A robust petro-elastic relationship obtained from rock physics models leads to more precise discrimination of pay and non-pay facies in the sand intervals of the study area. The Paleocene aged Lower Ranikot Formation and Pab sandstone of Cretaceous age are proven reservoirs of the Mehar gas field, Lower Indus Basin. These sands are widely distributed in the southwestern part of the basin and are enormously heterogeneous, which makes it difficult to distinguish facies and fluid content in the reservoir intervals. So, an attempt is made in this paper to separate the reservoir facies from non-reservoir facies by using an integrated approach of the petro-elastic domain in the targeted sand intervals. Furthermore, missing logs (S-sonic and P-sonic) were also synthesized in the wells and missing intervals along with improving the poor quality of the density log by captivating the washouts and other side effects. The calibrated rock physics model shows good consistency between measured and modelled logs. Petro-elastic models were predicted initially using petrophysical properties and incorporated at true reservoir conditions/parameters. Lithofacies were defined based on petrophysical cut-offs. Rock physics modelled elastic properties (Lambda-rho versus Mu-rho, impedance versus V_p/V_s ratio) were then cross-plotted by keeping lithofacies in the Z-axis. The cross-plots clearly separated and demarcated the litho-fluid classes (wet sand, gas sand, shale, and limestone) with specific orientation/patterns which were randomized in conventional petrophysical analysis.

Keywords: petrophysics, rock physics, cross-plots, Lambda-rho versus Mu-rho, impedance versus V_p/V_s ratio

1 Introduction

Exploration is the crucial step in the production planning of any petroleum industry which is considered to be an expensive, challenging, and time-consuming job. Estimation of probable facies along with other elastic rock properties is sufficiently required to reduce the risk and enhance the reliable data acquisition in any petroleum reservoir scenario [1–3]. Assessment of rock attributes such as lithology, texture, fluid saturation, porosity, and permeability is more challenging in clastic rocks due to their heterogeneous character [4,5]. The initial phase is to determine the best suitable parameters defining the complicated behavior of rocks. The heterogeneity comes due to primary and secondary minerals, pore texture, fluid type, porosity, pressure/temperature variations, and different formation processes [6]. These parameters mainly control the elastic properties which are being interpreted using a seismic data set. The conventional seismic interpretation provides a qualitative understanding of the geological structure and stratigraphic patterns with variations in density which is primarily controlled by velocity [7].

In the real world, geophysical observations can be predicted or interpreted in terms of rock properties by

* **Corresponding author: Urooj Shakir,** Department of Earth Sciences, Quaid-i-Azam University, 45320, Islamabad, Pakistan; Department of Earth and Environmental Sciences, Bahria University, Islamabad, 44000, Pakistan, e-mail: mhuroojshakir@gmail.com
Aamir Ali: Department of Earth Sciences, Quaid-i-Azam University, 45320, Islamabad, Pakistan
Muhammad Raiees Amjad: Department of Earth and Environmental Sciences, Bahria University, Islamabad, 44000, Pakistan
Muyyassar Hussain: Department of Earth Sciences, Quaid-i-Azam University, 45320, Islamabad, Pakistan; Advance Reservoir Characterization, LMK Resources, Sector I9/4, Islamabad, 44000, Pakistan

building a model of the rock that is consistent with the known data [8,9]. So, there is a need to find a potential model that links the geological properties and geophysical observations. For this, rock physics provides a bridge between well log and seismic to decipher the rock properties in elastic domain [10].

Rock physics is an interdisciplinary glue that plays a vital role and holds all the geoscience domains to fill the gaps present in each discipline and extract the core amount of rock information to draw a high-resolution picture of the reservoir [2,11]. This approach utilizes the concept of elastic properties measured from seismic data to predict rock attributes yielding the information about the reservoir rocks [12,13]. It also helps to quantify the sensitive reservoir properties of not only seismic data (e.g., velocity and seismic reflection amplitude), but also well log data of critical reservoir properties like porosity, lithology, pore fluid type, saturation, and pore pressure which are more vital for the quantitative analysis of a reservoir [14,15].

As well logs generally have temporal (vertical) resolution, quality of log data is more consistent and accurate at *in situ* so conditions and matters a lot to infer the true reservoir properties [16]. Petrophysical analysis of the zone of interest provides an insight to discriminate the fluid saturated and non-saturated reservoir intervals [17]. However, multiple factors such as missing log data, bad borehole conditions, mud cake, washouts, temperature, and salinity usually can affect the quality of log data leading to inaccurate petrophysical interpretation. Moreover, analysis of individual wells is reliable and consistent with the petrophysical interpretation of a particular zone, and hence, lacks in providing the interpolation of results between the wells in petro-elastic domain [18]. Here, the integrated petrophysics and rock physics modelling help to gain confidence in the quality of well log curves by comparing the difference between original (measured) and predicted (modelled) curves along with distinguishing the reservoir facies from the non-reservoir facies [19,20].

Rock physics modelling provides more accurate and reliable connection between seismic, petrophysics, and elastic reservoir properties [21,22]. Various authors have proposed a large number of rock physics models based on the particular mineral and reservoir conditions [23]. These models have been classified into different groups such as contact models, inclusion models, transformations, bounds, and computational models. The common log data required for these models are measured P-sonic (V_p), S-sonic (V_s), and density acquired during wireline logging [24,25]. As P-sonic and density are routinely acquired in wells as compared to S-sonic, main focus is given to shear sonic which is of pivotal importance in the success of these rock physics models. These logs (V_p, V_s and density) are either acquired from wireline logging or computed (V_s) from Greenburg and Castagna's equation during rock physics process. All three priorly stated logs are used to compute the bulk and shear moduli of rock, which further assists in estimating the fluid properties [26].

The quality of modelled shear sonic is controlled by comparing it with the existing models such as ref. [27] and theoretical ones such as ref. [28], or hybrid models such as [25,29–31]. Along with the other parameters, Mu-rho and Lambda-rho provide the additional information of the facies and fluid type because these are very sensitive to fluid prediction and categorization [19,32]. Once consistent rock physics modelled logs are available, petrophysical and elastic properties (V_p, V_s, Lambda-rho, Mu-rho) can not only be linked in a spurious way, but their output will also provide a robust way for reservoir properties estimation determined through seismic inversion [33].

The sands of Pab and Ranikot formations are proven targets in the Mehar gas field chosen as a study area in this research paper. These sand intervals are composed of quartz, clay, feldspar, and a minor amount of calcite [37]. Through well log and core data, it has been deduced that the mineral composition of these sands is very much heterogeneous from one well to another, creating difficulty in using a single petrophysical model for reservoir characterization [8,9].

This paper seeks to demonstrate the rock physics application to model the missing shear sonic and density log to enhance the relationship between petro-elastic properties and to demarcate the reservoir facies in an optimized way that will help in the prediction of lithology and fluid distribution over the entire volume. To accomplish this task, an integrated approach of petrophysics and rock physics modelling is adopted. Petrophysical analysis has been utilized to identify the reservoir intervals in the targeted formations, while rock physics helped out in prediction of missing log data and further to segregate the facies as output model based on P-sonic, S-sonic, Lambda-rho, and Mu-rho.

2 Geological information

Mehar gas field is located in south eastern part of the Kirthar Fold Belt (KFB) which is 150–200 km wide, north-south trending, east verging deformation zone [39,40]. It is

bounded by Kirthar foredeep in the east, Chaman Fault in the west, Sibi trough in the north, and Indus delta in the south (see Figure 1). The Kirthar foredeep is considered as a major kitchen for the generation of hydrocarbons in the KFB [34]. Lower Indus Basin is rich in hydrocarbon and several oil and gas fields were explored in the KFB, being host by Foredeep zone [35]. Late Cretaceous Pab Sandstone and Early Paleocene Lower Ranikot Formation (see Figure 2) are the primary target reservoirs in the southern KFB and hence in the study area [36]. The uplifting of the emergent Indian continent in the Early Cretaceous age triggered the deposition of sediments in the passive margin setting [37]. These sands were deposited in these environments which are acting as main reservoirs. These deposits are mainly of deltaic and shoreface origin having dominant unconsolidated sandstone, mixture of shale with some stringers of limestone. Organic rich shales of Mughalkot Formation, upper Cretaceous age, are the main source rock in the Mehar area. These shales are thermally matured and consist of type-III kerogen, making them more favorable for gas generation [38]. Great variations are observed in the depositional trend of the Pab sandstone and Lower Ranikot Formation from south to north. Pab sandstone majorly consists of thick clean sandstone beds with small striations of clay, while Ranikot consists of two parts, i.e., Lower Ranikot and Upper Ranikot Formation. Upper Ranikot is predominantly shale, while Lower Ranikot is composed of mixed carbonate-siliciclastic lithofacies, which can further be divided into three units in the study area. The lower division is carbonate-dominant towards the north and siliciclastic towards the south, the middle division is dominated by offshore muds and shale. At the same time, the upper-division contains sand units coarsening upward towards the north-northeast and is offshore mud dominated towards the south-southwest [39,40].

3 Methodology

3.1 Data used

For this project, data of three wells Mehar-01, Mehar-02, and Mehar-03 are utilized. All three wells penetrated the targeted Paleocene and Cretaceous reservoirs. Well data include complete log suites of gamma ray (GR), spontaneous potential (SP), calliper (CALI), sonic logs (DT4P, DT4S),

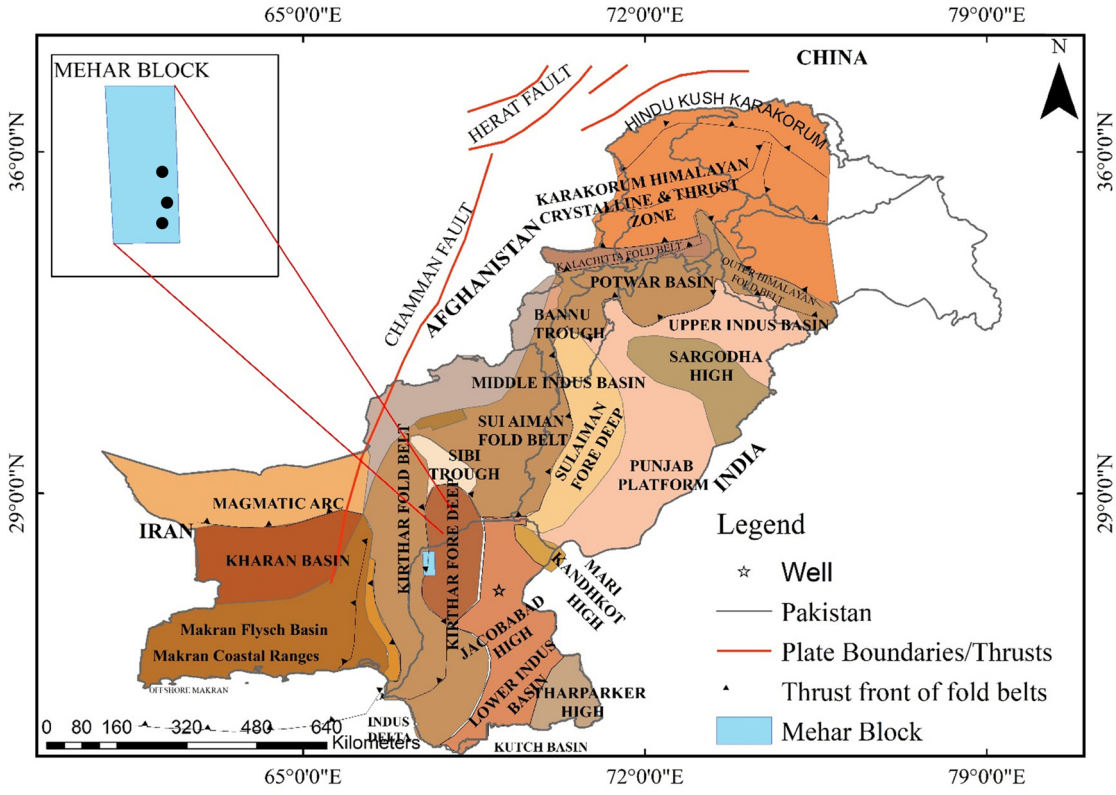

Figure 1: Map of the study area (Mehar Block). Blue rectangle in the tectonic map shows the cultural boundary of Mehar E&P lease with three wells (black dots) Mehar-01 (north), Mehar-02 (middle), and Mehar-03 (south) from north to south.

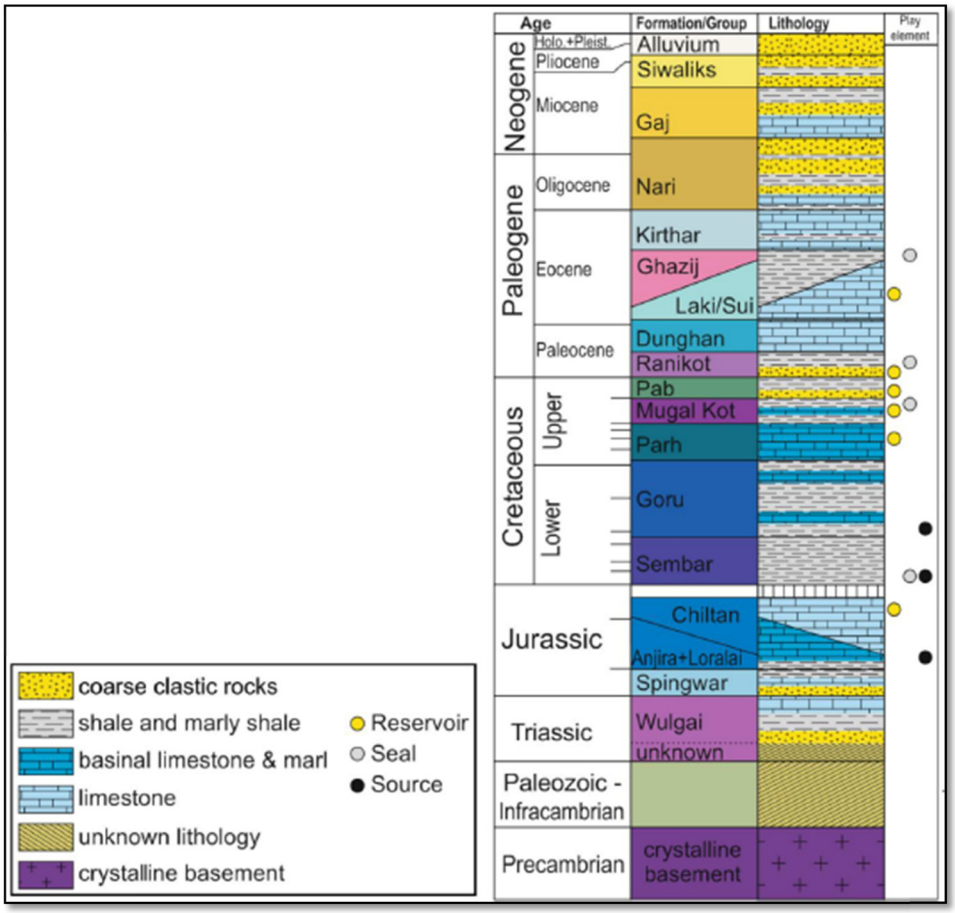

Figure 2: Generalized Stratigraphical column of Kirther Fold and Thrust Belt showing the lithostratigraphic overview and petroleum elements (Hinsch et al., 2018).

neutron porosity (NPHI), resistivity (MSFL, LLS and LLD), and density (RHOB) logs.

The adopted methodological scheme to carry out the work of petrophysics and rock physics is given below (see Figure 3).

3.2 Methodology

3.2.1 Petrophysics

Petrophysical interpretation provides insight for estimating the physical properties of the reservoir formations [41]. Formation evaluation and log facies are main parameters to link the rock properties with elastic (seismic) properties at the well locations [42]. In this study, detailed well log analysis is carried out using GVERSE petrophysics software to predict the reservoir characteristics utilizing the workflows presented by ref. [43] and [44,45]. The basic objective to perform well log interpretation is to identify the hydrocarbon-bearing sand intervals along with the porosity and fluid saturation [45]. More explicitly, the boundary of clean zones, estimation of petrophysical properties, and net payable thicknesses are calculated based on the criteria/formulae defined by the authors mentioned above.

Different logs with depth have been shown in the first four tracks like gamma ray, resistivity, and porosity along with the computed properties (porosity, lithology, and saturations) in the last four tracks from left to right. Correlation, resistivity, porosity, and track 4 have the input logs used for the petrophysical properties evaluation, while tracks 5, 6, 7, and 8 show the output properties computed using the equations (1)–(7) given below. Gamma ray log curve is used to differentiate between shaly and sandy lithology, while porosities were calculated using porosity (neutron and density) curves. Fluid saturation has been calculated by using resistivity curves. As Lower Ranikot Formation was having more shale content as compared to Pab Sandstone, water saturation was computed by applying both Archie's and Indonesian

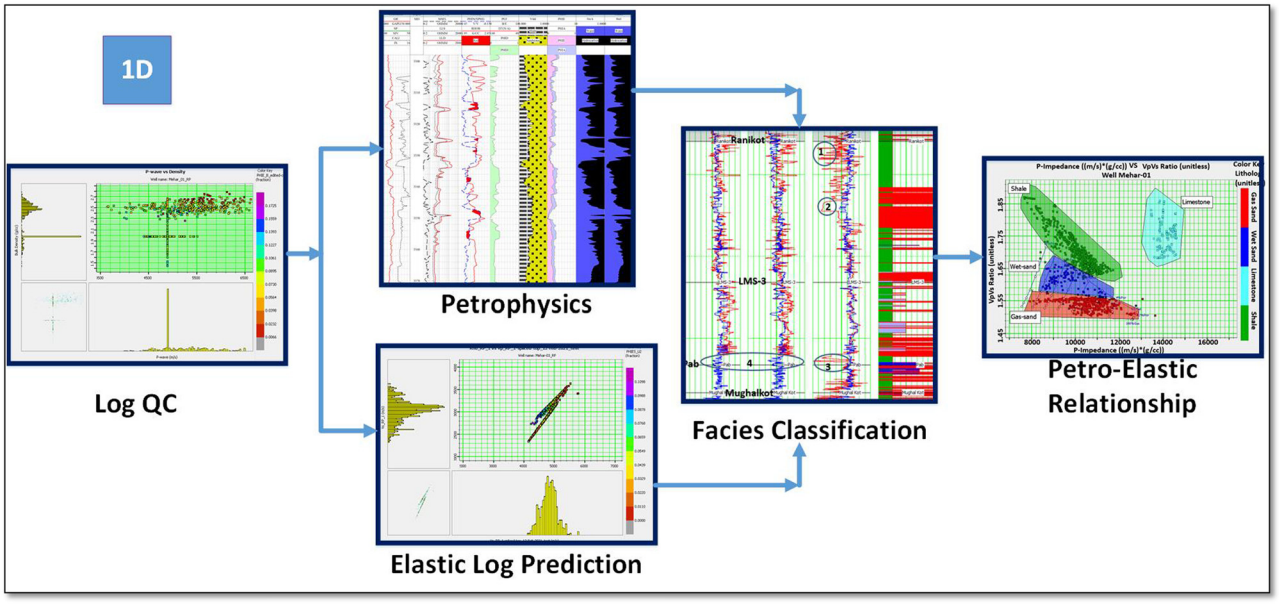

Figure 3: Schematic workflow adopted to perform rock physics modelling. Starting from quality checking the logs and involving the petrophysics and rock physics model to predict missing logs after removing the artifacts. Facies are well-resolved in the petro-elastic domain.

equations. Archie's equation includes the bound water and utilizes the resistivities for finding the water saturation, while the Indonesian equation removes the bound or irreducible water content which is associated with the clays and involves the volume of shale for water saturation along with the resistivity information. The petrophysical properties including volume of shale (equation (1)), average and effective porosities (equations (2)–(4)), saturation of water (equations (5) and (6)), and saturation of hydrocarbon (equation (7)) have been calculated for the three wells at the desired targeted depths by using the formulae taken from [46,47].

Volume of shale was calculated by using the formula given in equation (1)

$$V_{\text{shl}} = (\text{GR}_{\log} - \text{GR}_{\min})/(\text{GR}_{\max} - \text{GR}_{\min}), \tag{1}$$

where, V_{shl} is volume of shale; $\text{GR}_{\log}$ is gamma ray reading of formation; $\text{GR}_{\min}$ is minimum gamma ray (clean sand); and $\text{GR}_{\max}$ is maximum gamma ray (shale).

While for density porosity, formula given in equation (2) was utilized

$$\varphi_{\text{D}} = (\rho_{\text{m}} - \rho_{\text{b}})/(\rho_{\text{m}} - \rho_{\text{f}}), \tag{2}$$

where, ρ_{m} is density of matrix; ρ_{f} is density of fluid; ρ_{b} is log response in the zone of interest

Total porosity was calculated using equation (3)

$$\Phi_{\text{T}} = (\Phi_{\text{D}} + \Phi_{\text{N}})/2, \tag{3}$$

where, Φ_{T} is total porosity; Φ_{D} is density porosity; Φ_{N} is neutron porosity

Effective porosity was computed using the formula given below in equation (4)

$$\Phi_{\text{E}} = \Phi_{\text{T}}(1 - V_{\text{sh}}), \tag{4}$$

where, Φ_{E} is effective porosity; Φ_{T} is total porosity; V_{sh} is volume of shale

The formula used for calculating water saturation using Indonesian equation (5):

$$S_{\text{w Indonesia}} = \left\{ \frac{\sqrt{\frac{1}{R_{\text{t}}}}}{\left(\frac{V_{\text{sh}}^{(1-0.5V_{\text{sh}})}}{\sqrt{R_{\text{sh}}}}\right) + \sqrt{\frac{\phi_{\text{e}}^{m}}{a \cdot R_{\text{w}}}}} \right\}^{(2/n)}, \tag{5}$$

where, S_{w} is water saturation (Indonesian); R_{t} is deep resistively; R_{w} is the resistivity of the formation water; V_{sh} is volume of shale; R_{sh} is resistivity of shale; Φ_{e} is effective porosity; n is the saturation exponent; and m is the cementation exponent

Water saturation using Archie's equation (6) is given by

$$S_{\text{w}} = \sqrt[\frac{1}{n}]{\frac{F \times R_{\text{w}}}{R_{\text{t}}}}, \tag{6}$$

where, R_{w} is water resistivity; R_{t} is true resistivity; n is saturation exponent and with value 2; F is formation factor $\left(\frac{a}{\varphi^{m}}\right)$; a is tortuosity factor with value; φ is effective porosity; m is cementation factor with a constant value 2. All the factors of Archie's equation are calculated from well header information. After calculating water saturation, saturation of hydrocarbon was computed using formula

given below because sum of the two saturations is 100%, so following equation (7) formula gives the hydrocarbon saturation

$$S_h = 1 - S_w, \tag{7}$$

where, S_h is saturation of hydrocarbon; S_w is saturation of water.

3.2.2 Rock physics

In each well, Pab and Ranikot formations have been targeted and interpreted. In Mehar-01 well, P-sonic and S-sonic are missing in the lower part of the reservoir, while a poor-quality density log is present in the whole zone. Mehar-02 well contains complete coverage of P-sonic and density log while missing S-sonic. Initially, the Shear sonic log is generated using [27] relationship and later modelled to optimize it. The splice zone is also present in the P-wave in Mehar-02 in the reservoir depth. Mehar-03 well contains a complete suite of elastic and petrophysics logs restricted to reservoir zone only. The data quality of the density log is comparatively poor in all three wells due to washed out zones. Preliminary data (de-spiking) conditioning and depth matching have been performed earlier. The source wavelet utilized was a statistical wavelet extracted from seismic data with a frequency range from 5 to 30 Hz having a constant zero phase. Initially, density and p-wave measured (raw) logs were convolved for synthetic generation. Later, modelled logs after rock physics application were utilized for synthetic generation. Finally, the two synthetics obtained were compared to analyze the best correlation. Synthetic generated using modelled logs showed a much better correlation as compared to synthetics generated using measured (raw) logs. Both the logs have been shown in the Figure 6a–c with blue (modelled) and red (measured) colors.

Rock physics analysis has been carried out by using the RockSI utility of HampsonRussell Software. According to [48], rock physics analysis requires four main components: minerals, fluids, the rock frame, and their assemblage (see Figure 4). In this study, the initial framework for the

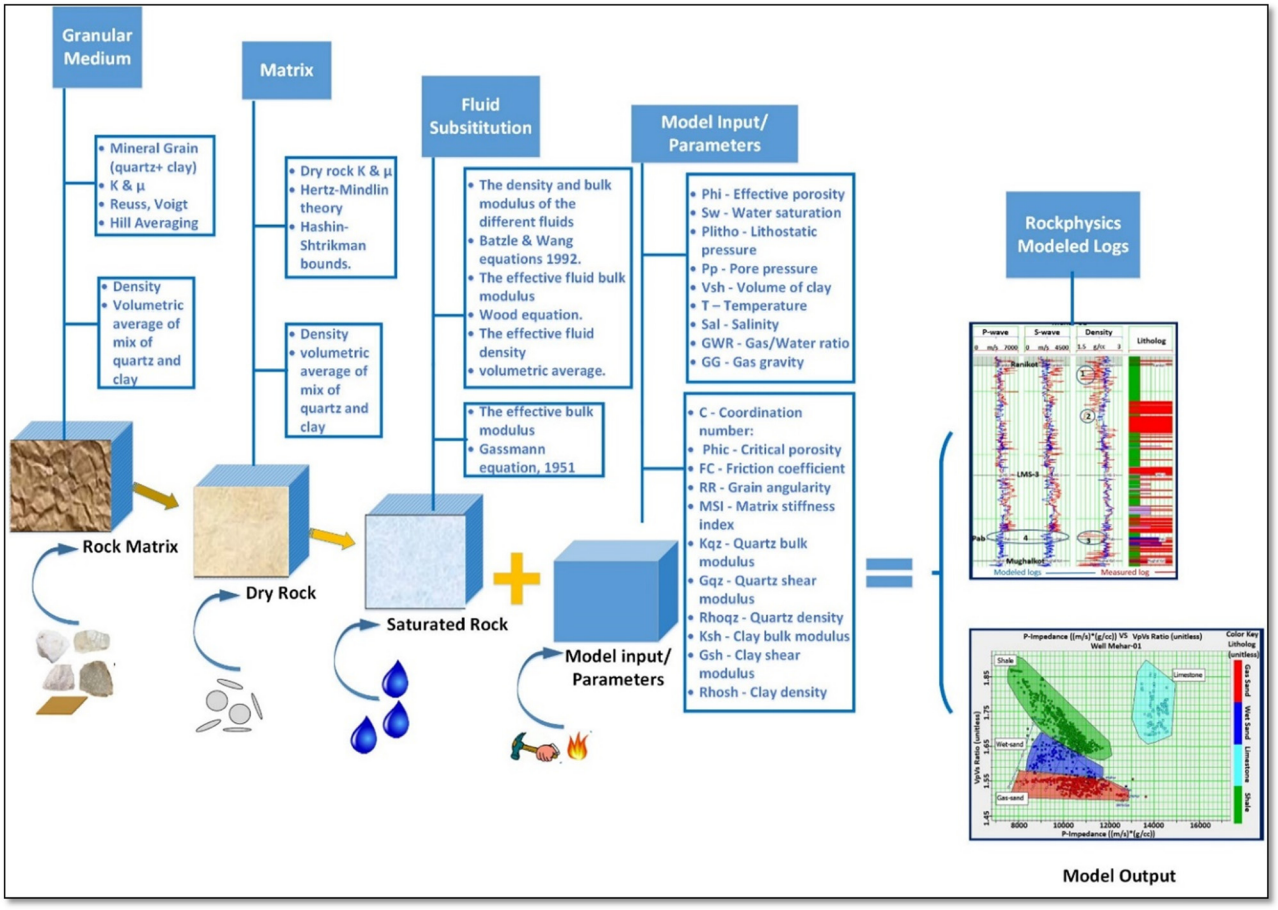

Figure 4: Granular model is established by incorporating rock matrix in the dry rock frame which later is saturated by fluids using model inputs/parameters. Adopted workflow utilized to perform rock physics modelling.

unconsolidated sandstone model, saturated with brine and gas, is utilized using equation (8), where the Ruess-Voigt equation [49] is used to compute the elastic moduli, while density is computed as their volumetric average.

The pressure-dependent effective dry rock bulk and shear moduli are computed with Hertz-Mindlin contact theory [31] at the critical porosity. The lower Hashim-Shtrikman lower bound [28] is applied here for an unconsolidated sand reservoir.

$$\frac{1}{K_{\mathrm{m}}} = \frac{V_{\mathrm{shale}}}{K_{\mathrm{shale}}} + \frac{(1 - V_{\mathrm{shale}})}{K_{\mathrm{quartz}}}, \tag{8}$$

where, K_{m}, K_{shale}, and K_{quartz} are bulk moduli of matrix, shale, and quartz, while V_{shale} is volume of shale

Then dry rock moduli (equation (9)) at effective pressure and critical porosity were computed using Hertz-Mindlin theory using the formula given below. Dry rock moduli using Hashin-Shtrikman bounds were also computed over a range of porosities [45]. Both upper and lower bounds were applied to see the compaction and cementation trends.

$$\frac{1}{K_{\mathrm{dry}}} = \frac{1}{K_{\mathrm{m}}} + \frac{\varphi}{K_{\varphi}}, \tag{9}$$

where, K_{dry} is bulk modulus of dry rock frame; K_{m} is bulk modulus of matrix; K_{φ} is bulk modulus at given porosity; and φ is porosity.

Afterward, Gassmann's fluid substitution for saturated rock frame was performed using equations (10) and (11) and moduli were calculated by assuming that the pore spaces are fully saturated with the fluids. The shear moduli of dry and saturated are same.

$$\frac{1}{K_{\mathrm{sat}}} = \frac{1}{K_{\mathrm{m}}} + \frac{\varphi}{\tilde{K}_{\varphi}}, \quad \tilde{K}_{\varphi} = K_{\varphi} + \frac{K_{\mathrm{m}} K_{\mathrm{f}}}{K_{\mathrm{m}} - K_{\mathrm{f}}}, \tag{10}$$

$$G_{\mathrm{sat}} = G_{\mathrm{dry}}, \tag{11}$$

where, K_{sat}, K_{m}, $\tilde{K}_{\varphi}$, and K_{f} are bulk moduli while G_{sat} and G_{dry} are shear moduli of saturated rock, matrix, porosity at given temperature, and fluid, respectively.

Elastic parameters of fluids used in the models have been shown in Table 1.

Batzle & Wang's [50] equations are used to compute the density and bulk modulus of the different fluids, while the effective fluid density and bulk modulus are derived using volumetric average and Wood's equation given in equations (12) and (13), respectively.

$$\rho_{\mathrm{sat}} = \rho_{\mathrm{matrix}} (1 - \varphi) + \rho_{\mathrm{fluid}} \varphi, \tag{12}$$

$$\rho_{\mathrm{fluid}} = \rho_{\mathrm{water}} S_{\mathrm{water}} + \rho_{\mathrm{gas}} S_{\mathrm{gas}}, \tag{13}$$

where, ρ_{sat}, ρ_{matrix}, and ρ_{fluid} are densities of saturated rock, matrix, and fluid, respectively. Finally, velocities of P and S waves at saturated rock conditions are calculated using the formulae given below in equations (14) and (15), respectively.

Table 1: Elastic, and PVT properties at Reservoir Interval (Babasafari et al., 2020)

Mineral/ Fluid	Density (g/cc)	Bulk modulus (GPa)	Shear modulus (GPa)
Quartz	2.65	37	45
Clay	2.6	15	5
Coal	1.8	6	1.5
Water	1	2.46	0
Oil	0.75	1	0
Gas	0.1	0.02	0
Oil gravity	30API		
Gas gravity	0.6		
Pressure	2500PSI		

$$V_{\mathrm{P\_sat}} = \sqrt{\frac{K_{\mathrm{sat}} + 4/3\, G_{\mathrm{sat}}}{\rho_{\mathrm{sat}}}}, \tag{14}$$

$$V_{\mathrm{S\_sat}} = \sqrt{\frac{G_{\mathrm{sat}}}{\rho_{\mathrm{sat}}}}, \tag{15}$$

where, K_{sat} and G_{sat} are bulk and shear moduli of saturated rocks, respectively.

Model input reservoir conditions including temperature, pore and litho-static pressures, brine salinity, gas water ratio (GWR), and gas gravity are taken from the core and well log reports (see Table 1), while calculated petrophysical properties including effective porosity (Phie), shale volume (V_{sh}), and water saturation (S_{w}) have been used from petrophysical analysis (see Table 2). The model parameters including coordination number (C), critical porosity (Phic), friction coefficient (FC), grain angularity (RR), and matric stiffness index (MSI) along with the density, bulk, and shear moduli for quartz and clay have been optimized iteratively to match the model logs with the measured logs and then P-sonic, S-sonic, and density have resulted. Afterward, the rock physics template was overlaid on the cross-plots generated in the petro-elastic domain.

4 Results

4.1 Petrophysics

Petrophysical analysis has been performed on selected zones of Pab sandstone and lower Ranikot formations

Table 2: Petrophysical properties of the reservoir zones in the wells Mehar-01, 02, and 03

Well name	Shale volume (%)	Effective porosity (%)	Water saturation (%)
		Mehar-01	
Lower Ranikot	30	17	40
Pab	17	15	35
		Mehar-02	
Lower Ranikot	18	12	15
Pab	19	15	15
		Mehar-03	
Lower Ranikot	20	12	30
Pab	18	10	40

in the three wells Mehar-01, 02, and 03. The reservoir intervals have been chosen after applying zones of interest criteria (low gamma ray value, Separation between LLD and MSFL, cross over between Nphi and RhoB) and cut-off values (volume of clay >30%, water saturation ≥50%, and volume of calcite >60%) shown in Table 3. The petrophysical properties calculated have been shown in the last four tracks with lithology, porosity, and saturation. Pab sandstone is cleaner and has less clay content as compared to the lower Ranikot Formation. The porosity behavior is almost same for both formations having an average value between 12 to 15%, shale volume 17 to 20% on average, and water saturation 20 to 35% on average. The petrophysical analysis revealed that the upper part of the Ranikot Formation is not favorable for hydrocarbon production in any well as it exhibits a high volume of shale (V_{sh}) (33%), low effective porosity (Phi) (6%), high water saturation (S_w) (70%), and false crossover between density and neutron porosity logs, while the Pab sandstone has shown more promising character in the three evaluated wells with the high effective porosities and saturations. Good effective porosity, less volume of clay, and high saturations for the lower part of the Lower Ranikot make it more economically viable especially for well Mehar-02 (Table 2). Petrophysical interpretation of Pab and Lower Ranikot formations of well 03 has been shown in Figure 5a and b. The quantitative values of reservoir properties in both the formations of three wells are mentioned in Table 2. These calculated rock attributes have been utilized further in the rock physics analysis as an input parameter along with the other properties.

4.2 Rock physics modelling

The data quality of the measured and predicted elastic logs P-sonic, S-sonic, and density in all three wells (Mehar-01, 02 & 03) is quite evident in Figure 6a–c. At the depth from 3,235–3,675 m, 3,805–3,965 m, and 3,710–3,868 m in wells 01, 02, and 03, respectively, multiple sand intervals are acting as a reservoir due to low shale volume, good porosities, and low water saturation. Splice zones observed in the measured logs are highlighted by blue circles and ovals in Figure 6a–c. The first three columns having V_p (1st column), V_s (2nd column), and density (3rd column) show a good match between the rock physics modelled logs (red) with the measured/conditioned logs (blue), while the reservoir zone consists of multiple facies containing gas sand (red), wet sand (blue), shales (green), and carbonates (sky blue) shown as a litho-log in the last column (see Figure 6a–c). These facies are classified based on the ranges defined in estimating petrophysical properties using equations (1)–(7) (see Table 3).

4.3 Mu-rho and Lambda-rho cross-plot analysis

The cross-plots of measured and predicted Mu-rho and Lambda-rho elastic properties are shown below (see Figures 7–9). As Mu-rho and Lambda-rho are very sensitive towards fluids and lithology, the Lamé's parameters, rigidity (μ) and lambda (λ), were utilized for the discrimination of brine

Table 3: Facies classification criteria based on petrophysical properties

Facies name	Well log	Lower limit	Upper limit	Facie color
Shale	Volume of clay	>30%	Nil	Green
Carbonates	Volume of calcite	>60%	Nil	Sky blue
Wet sand	Water saturation	≥50%	Nil	Blue
	Volume of clay	Nil	≤30%	
Gas sand	Water saturation	Nil	<50%	Red
	Volume of clay	Nil	≤30%	

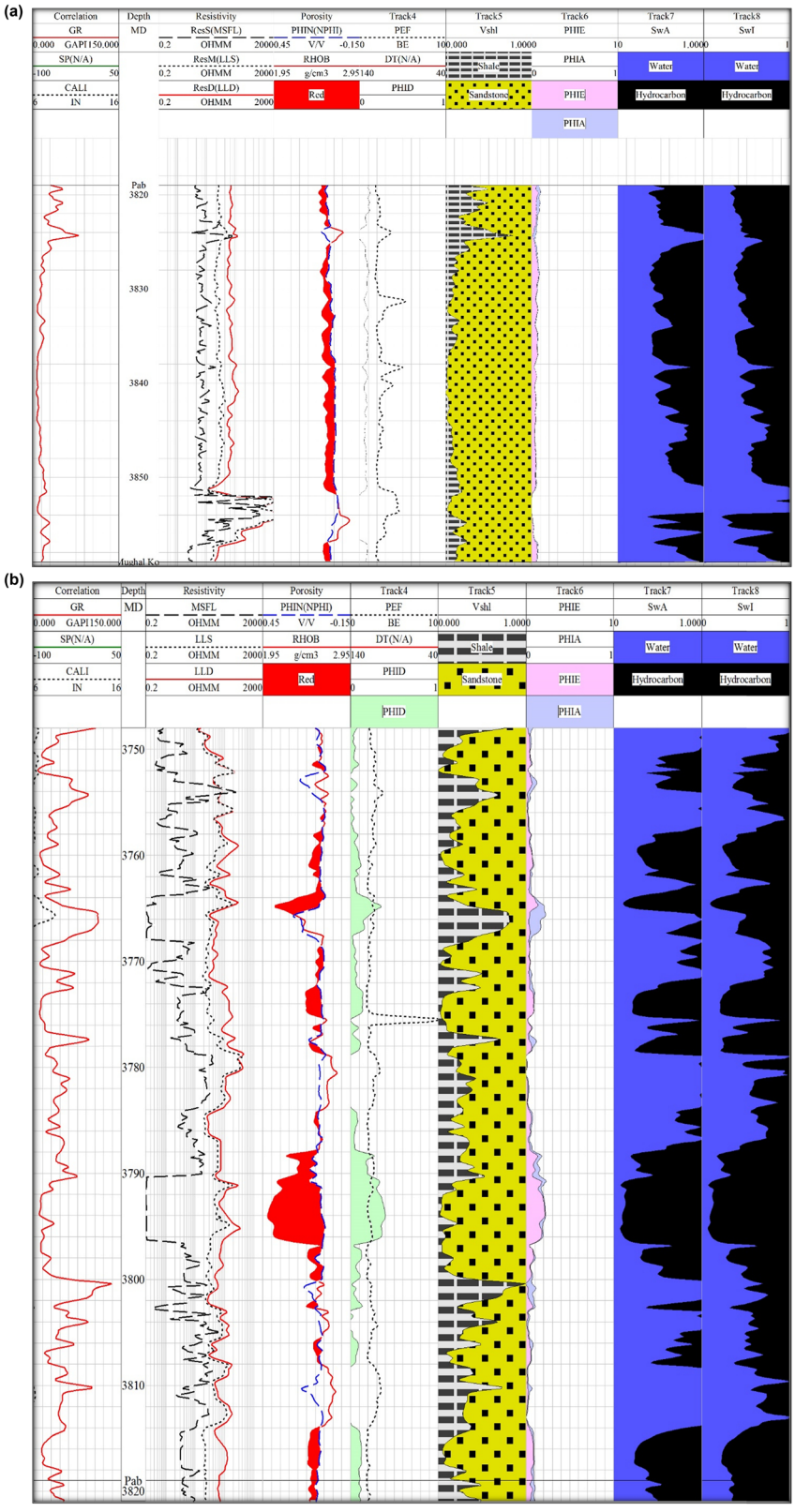

Figure 5: (a) Petrophysical analysis done on the complete reservoir interval of the Cretaceous sand (Pab) in well M-03. Calculated rock properties are shown along with the logs in multiple tracks from left to right. (b) Petrophysical analysis done on the reservoir interval of the Paleocene sand (Lower Ranikot) in well M-03. Calculated rock properties are shown along with the logs in multiple tracks from left to right.

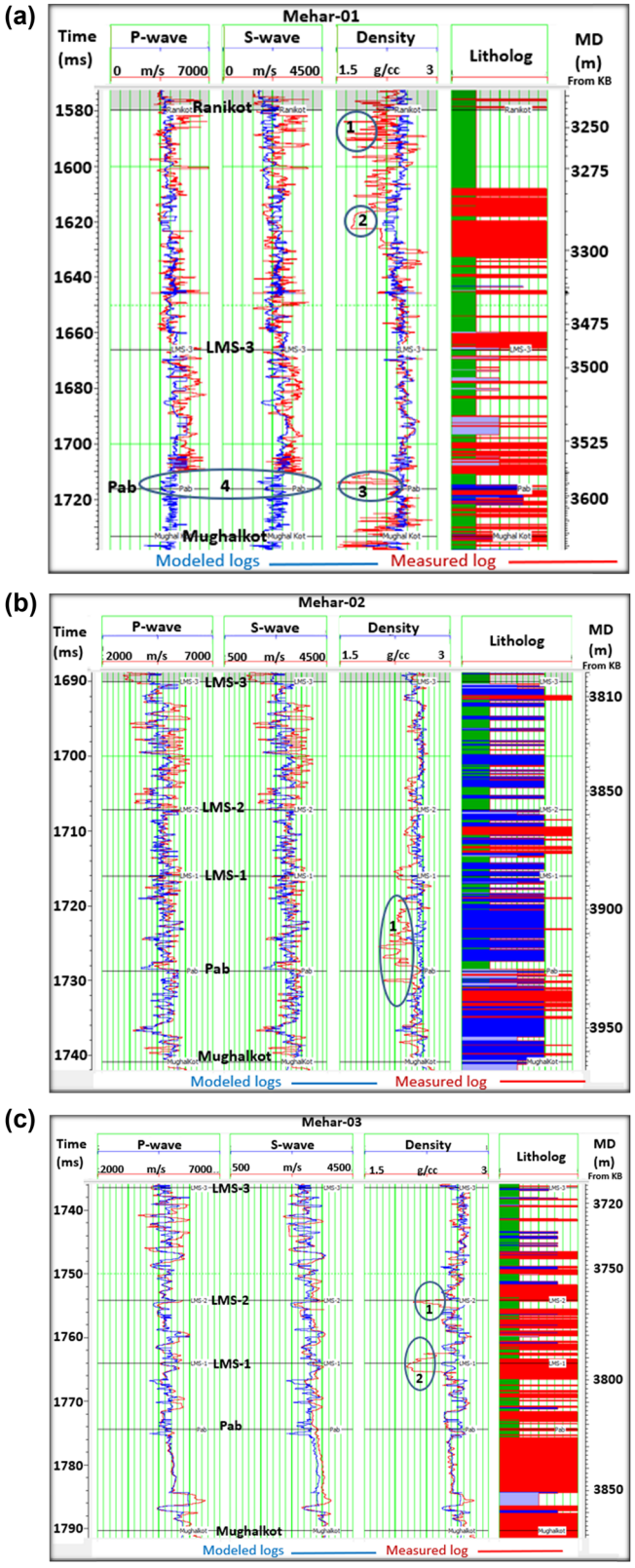

Figure 6: (a) P, S, and density logs quality with rock physics modelled logs (blue) and measured logs (red) in Maher-01 well. Spiking behavior of curve has been removed after rock physics modelling (circle 1). Bad density log conditions due to rouges hole have been improved after modelling shown in circle 2 and oval 3. Missing P and S logs in the lower part of well have been successfully modelled (oval 4). (b) P, S, and density logs quality with rock physics modelled logs (blue) and measured logs (red) in Maher-02 well. Bad density log conditions due to rouges hole have been improved after modelling (oval 1). (c) P, S, and density logs quality with rock physics modelled logs (blue) and measured logs (red) in Maher-03 well. Bad density log condition due to rouges hole has been improved after modelling (oval 1 & 2).

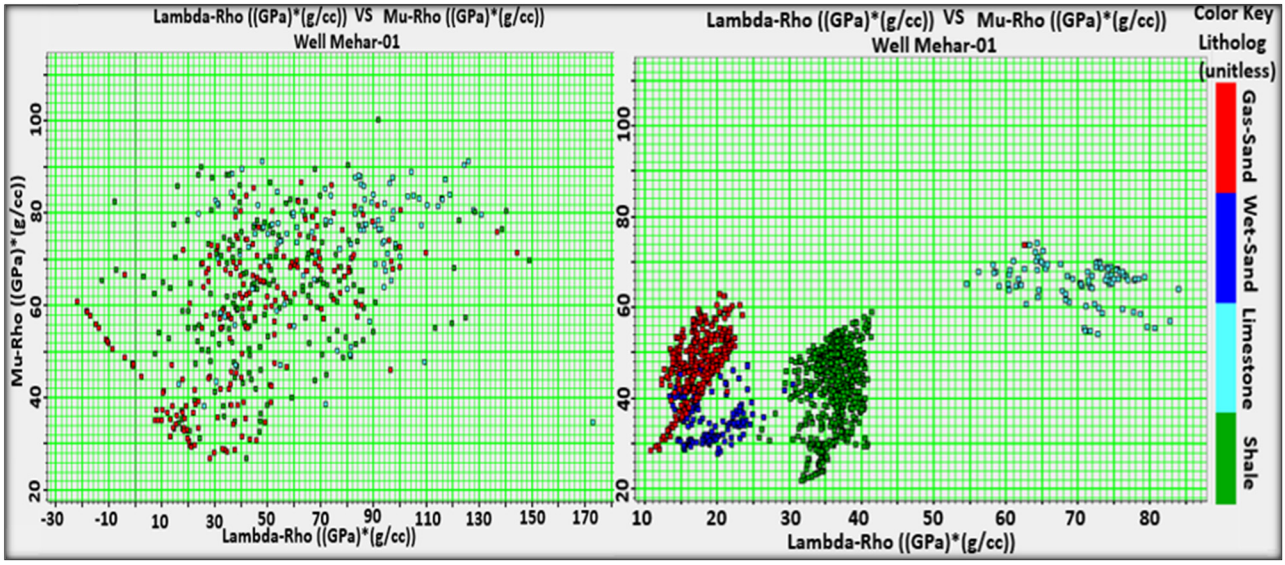

Figure 7: Rock physics modelled cross-plot of Lambda-Rho versus Mu-Rho for reservoir interval, clearly demarcating the gas sand, wet sand, limestone, and shale in Mehar-01 well in the right cross-plot. Measured logs are plotted in left cross-plot where separation between the facies is obscured.

sand from hydrocarbon-bearing sand. Lambda (incompressibility) is a P-wave-derived parameter and is more sensitive for lithology prediction. Since fluids show resistance against compression, their presence and saturation lead to a significant reduction in the incompressibility measurement. Lamda-rho, thus being a product of lambda with bulk density, is a good lithology indicator. As hydrocarbon-bearing sand is denser than water-filled sand, low values of Lambda-rho show a good gas sand effect [51,52].

Mu (rigidity), on the other hand, is a shear wave-derived parameter. As sand is more rigid than shale, it exerts more resistance to shearing. Mu alone is not mainly affected by fluid type, so its values in hydrocarbon and brine sand most likely remain relatively constant. Mu-rho, thus being the product of Mu with bulk density, is a good fluid indicator with high values being consistent with gas sand [53].

In every cross-plot, Lambda-rho is kept on *X*-axis, while Mu-rho is plotted on *Y*-axis with the lithological facies on *Z*-axis within the reservoir zone. There is no pattern/orientation observed for facies in the elastic measured domain, rather few abnormal patterns are present

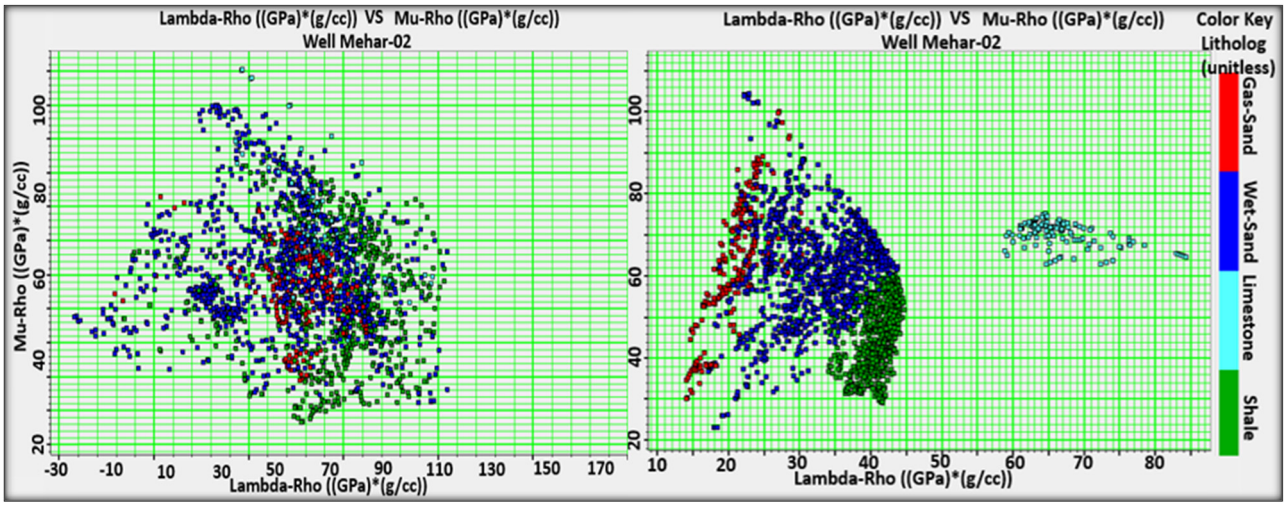

Figure 8: Rock physics modelled cross-plot of Lambda-Rho versus Mu-Rho for reservoir interval, clearly demarcating the gas sand, wet sand, limestone, and shale in Mehar-02 well in the right cross-plot. Measured logs are plotted in left cross-plot where separation between the facies is obscured.

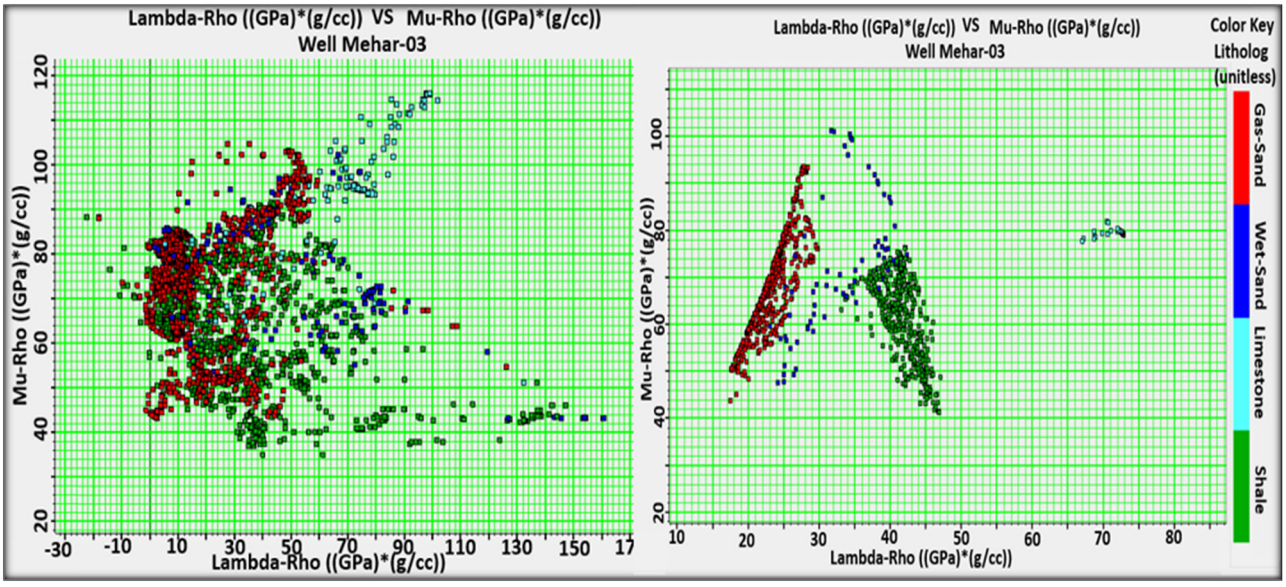

Figure 9: Rock physics modelled cross-plot of Lambda-Rho versus Mu-Rho for reservoir interval, clearly demarcating the gas sand, wet sand, limestone, and shale in Mehar-03 well in the right cross-plot. Measured logs are plotted in left cross-plot where separation between the facies is obscured.

in the measured logs. Since well log data are considered to be affected by many parameters and borehole conditions, it is difficult to discriminate lithology and fluid content from elastic log data alone. Furthermore, it is unable to separate particular facies in measured petro-elastic domain, thereby missing the prior relationship that is the core step for reservoir characterization. Thus, the rock physics template needs to be taken into account along with the modelled elastic properties to reduce risk for the interpretation. In the predicted logs, input parameters are well-controlled, making it more reliable and effective to discriminate different types of facies. The cross-plots with measured logs parameters (left) and improved modelled logs (right) are shown in the Figures 7–9 for the wells Mehar-01, 02, and 03, respectively, and for combined wells (see Figure 10), depicting proper facies orientation with clear demarcation between the pay and non-pay facies.

The predicted cross-plots defined four facies present in the reservoir interval. Zone with medium Mu-rho and high Lambda-rho corresponds to the limestone facies (sky blue cluster points), while the zone with low to moderate Mu-rho and moderate Lambda-rho values depicts shale facies occurrence (green cluster points). Low to medium Lambda-rho and Mu-rho values are defined as brine sand (blue cluster points), whereas low to medium Mu-rho with very low Lambda-rho values represents typical of a gas sand (red cluster points). In conclusion, Lambda-rho on the horizontal axis provided good separation of the shale, limestone, wet sand, and gas sand facies, which is a typical lithological indicator. Hence, rock physics modelled logs with the above said attributes helped to clearly differentiate the objective facies. Hence, Lame's parameters are effectively used to characterize lithology and fluid for prospect evaluation.

4.4 Impedance versus V_p/V_s ratio cross-plot analysis

Rock properties such as acoustic impedance and V_p/V_s ratio also play a vital role to separate hydrocarbon saturated facies from the rest of non-pay facies. Cross-plots of P-imp and V_p/V_s ratio are generated overlain by rock physics template with facies displayed on the Z-axis for the three wells (see Figures 11–13). Four zones/clusters of facies are clearly separated on these cross-plots. The points with low acoustic impedance (1,000–14,000 m/s*g/cc), low V_p/V_s (1.52–1.57), high porosity, and high gas saturation depict the gas sand facies highlighted in red polygon [31,54]. However, green polygon with high values of V_p/V_s ratio, water saturation (100% saturation), and impedance represents shale facies without gas saturation. The area lying between the two separated zones (sand and shale) is an indicator of water saturation. These wet sands highlighted by blue polygon are showing relatively high values of impedance and water saturation compared to gas sand. The high P-impedance and moderate to high V_p/V_s ratio exhibit limestone highlighted by sky blue color

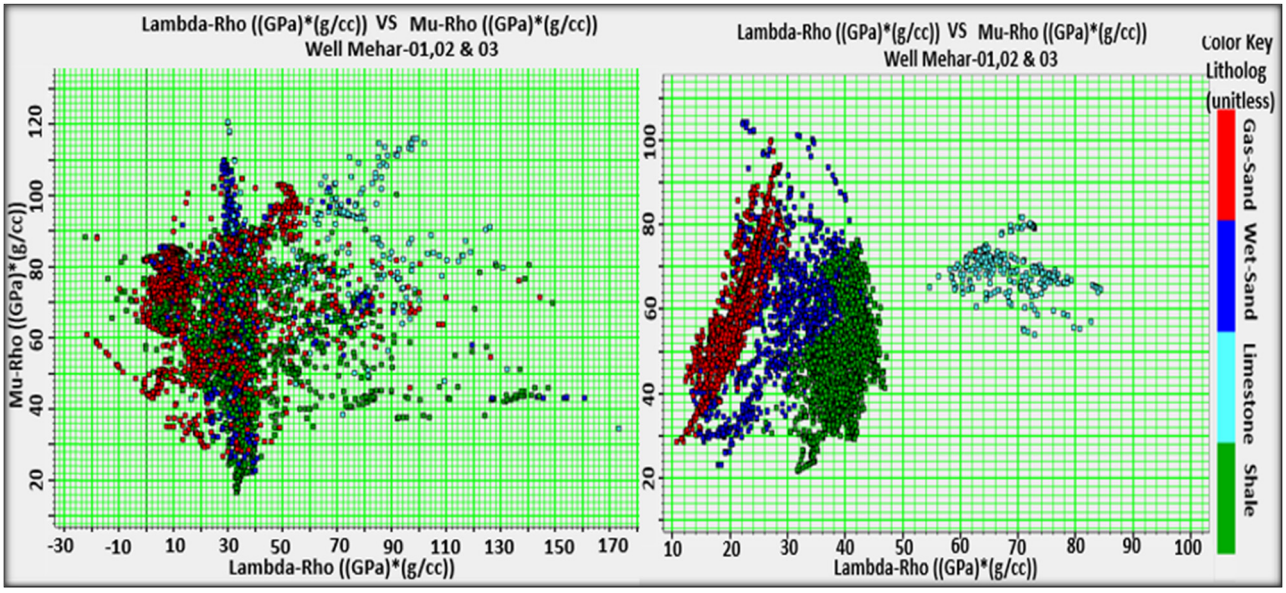

Figure 10: Rock physics modelled cross-plot for combined wells of Lambda-Rho versus Mu-Rho for reservoir interval, clearly demarcating the gas sand, wet sand, limestone, and shale after rock physics modelling in the right cross-plot. Measured logs are plotted in left cross-plot where separation between the facies is obscured.

polygon. The facies segregated through different polygons are clearly demarcating the similar facies present in the litho-log shown previously (see Figure 6a–c) for the three wells in the reservoir zone.

Figures 14–16 show the comparison of well to seismic tie between the measured and modelled logs and an improvement in seismic-synthetics correlation was observed. The correlation coefficient calculated using measured logs is 64, 75, and 73% at well Mehar –01, 02, and 03, respectively (see Figures 14a–16a). This coefficient improved robustly after using modelled logs reaching up to 82, 80, and 88% for the above said wells (see Figures 14b–16b).

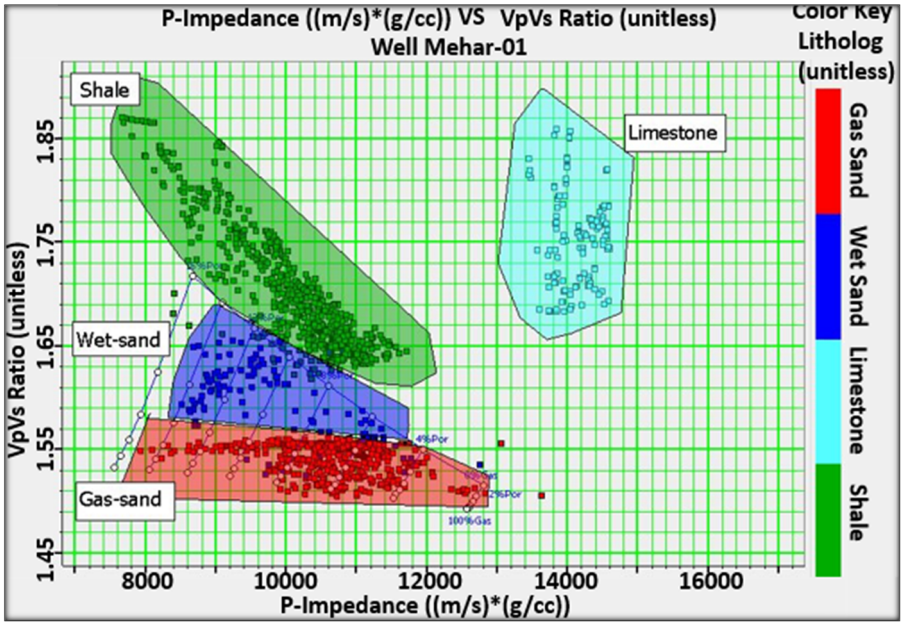

Figure 11: Rock physics modelled logs cross-plot of V_p/V_s ratio versus impedance for reservoir depicting a clear demarcation between gas sand, wet sand, limestone, and shale in Mehar-01 well overlain by rock physics template, i.e., showing the behavior of porosity and saturation trends.

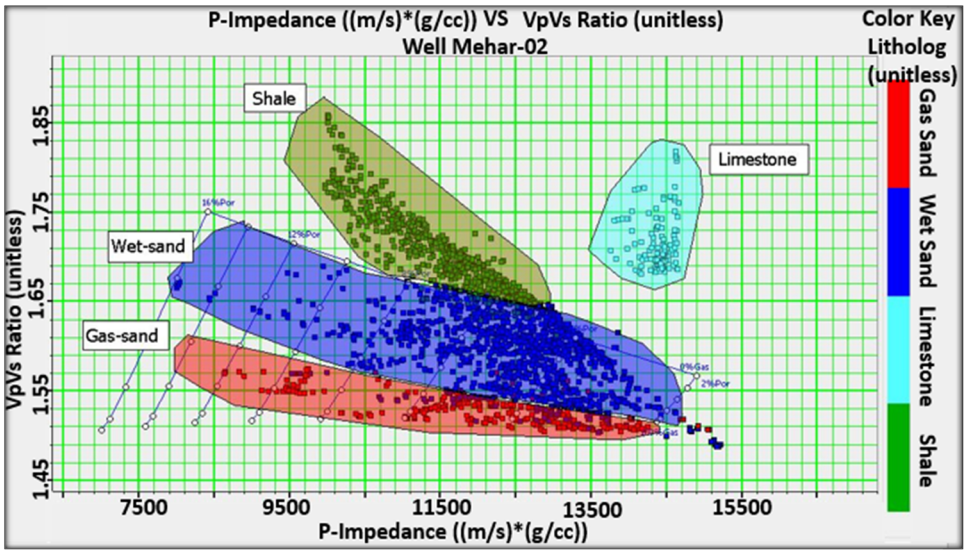

Figure 12: Rock physics modelled logs plot of V_p/V_s ratio versus impedance versus for reservoir depicting a clear demarcation between gas sand, wet sand, limestone, and shale in Mehar-02 well overlain by rock physics template, i.e., showing the behavior of porosity and saturation trends.

5 Discussion

An integrated approach of petrophysics and rock physics is utilized in this paper to characterize the reservoir properties in the elastic domain that can absolutely differentiate the pay facies from the non in the Mehar Gas Field of the Central Indus Basin, Pakistan.

The technique applied in this paper can easily be adopted to segregate the pay and non-pay facies in the basins having the complex and heterogenous clastic rocks. Magoba and Opuwari [18] classified facies and hydrocarbon prospects in shallow marine sandstone, offshore south Africa, using petrophysics and fluid substitution modelling. Likewise, Yasin et al. [55] performed rock

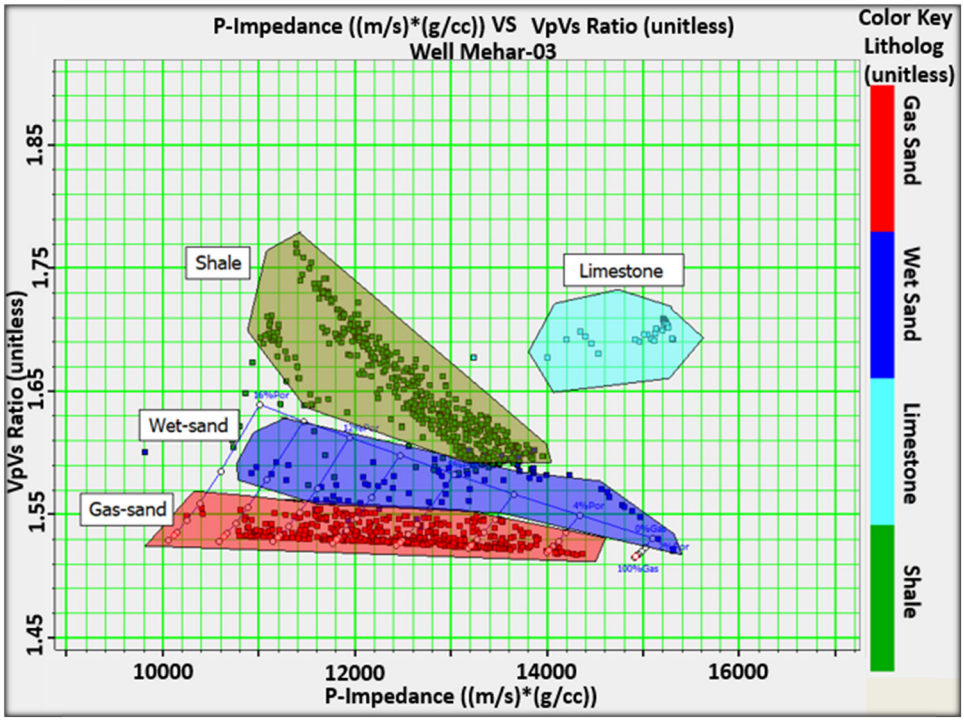

Figure 13: Rock physics modelled logs plot of V_p/V_s ratio versus impedance versus V_p/V_s Ratio for reservoir depicting a clear demarcation between gas sand, wet sand, limestone, and shale in Mehar-03 well overlain by rock physics template, i.e., showing the behavior of porosity and saturation trends.

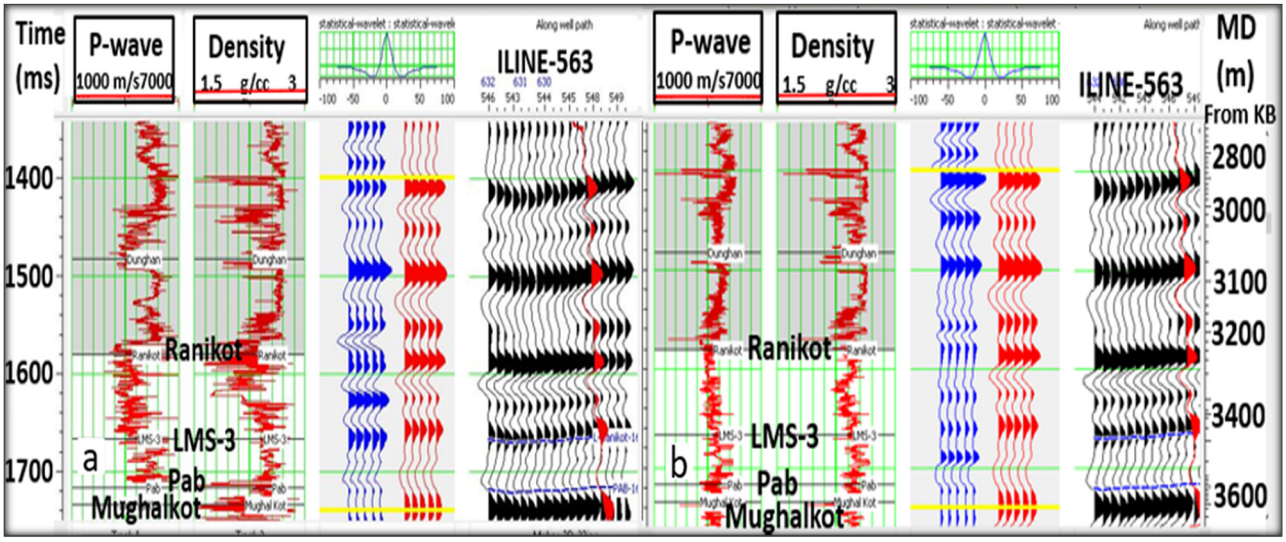

Figure 14: In Mehar-01 well, synthetic seismogram has been generated using measured logs on the left plot (a). In the right plot (b), synthetic seismogram has been generated using rock physics modelled logs where along with the improvement in the quality of logs, well to seismic correlation coefficient is also improved.

physics analysis to develop a relationship between elastic and petrophysical properties using inversion technique to classify extremely heterogeneous clastic reservoirs rocks. An integrated approach of petrophysics and rock physics has been applied in the gas field of lower Indus basin by Azeem et al. [9] by integrating petrophysics and rock physics to characterize cretaceous sand intervals. Fitch et al. [56] suggested that rock physics modelling technique is suitable to bridge the gap between core and seismic data to enhance the hydrocarbon facies.

The adopted methodology assisted in developing a consistent and reliable rock physics model. In the initial phase, well log interpretation was carried out to highlight the targeted reservoir zones in the used wells. The calculated petrophysical properties were then used as an input to build the rock physics models. The predicted logs were in good match and acceptable range with the measured elastic logs. Moreover, litho-fluid facies were efficiently differentiated with the modelled cross-plots. The prior information of core, geology, and well logs helped to

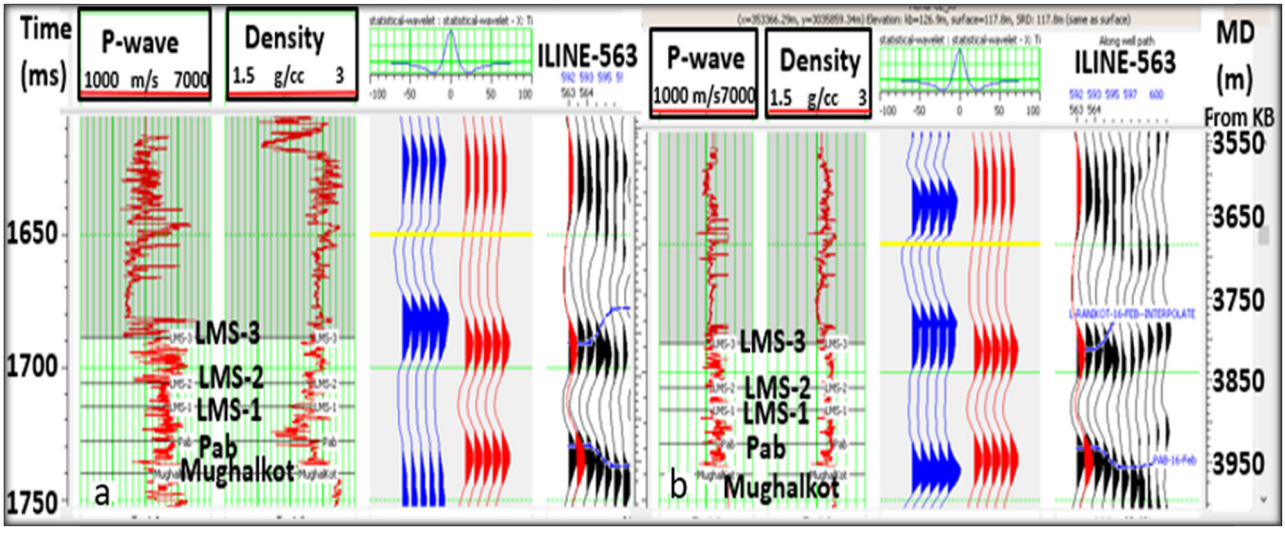

Figure 15: In Mehar-02 well, synthetic seismogram has been generated using measured logs on the left plot (a). In the right plot (b), synthetic seismogram has been generated using rock physics modelled logs where along with the improvement in the quality of logs, well to seismic correlation coefficient is also improved.

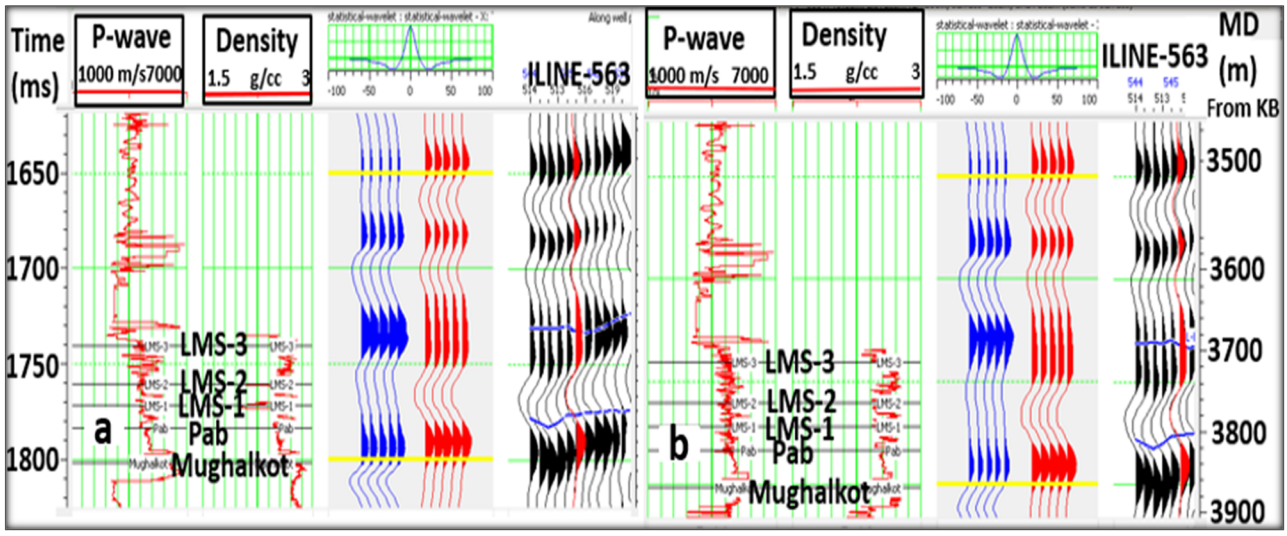

Figure 16: In Mehar-03 well, synthetic seismogram has been generated using measured logs on the left plot (a). In the right plot (b), synthetic seismogram has been generated using rock physics modelled logs where along with the improvement in the quality of logs, well to seismic correlation coefficient is also improved.

build the rock physics template with the inclusion of fluid type, pressure, and temperature conditions. The predicted model proved fruitful not only in accurate estimation of true elastic parameters (V_p, V_s, density), but also helped to model S-sonic log in that well where it is missing in the targeted zones. Furthermore, washout and spiking effects were removed from the measured density log. Cross-plots of Mu-rho, Lambda-rho, Impedance, and V_p/V_s ratio efficiently segregated the fluid-filled facies from the water saturated and shale facies. Based on cross-plots analysis, the quantitative values of elastic parameters have been defined to differentiate between the gas sand, shale, wet sand, and limestone. As the Mu-rho is sensitive towards fluids, they provided good separation of gas sands on the *Y*-axis, while Lambda-rho on the *X*-axis effectively segregated the lithological facies. On the other hand, V_p/V_s ratio is more sensitive to gas-bearing sand accompanying the impedance. Moreover, the modelled logs helped to improve the well to seismic tie that improved the reservoir characterizations in a better way. Thus, rock physics modelled logs provided a robust way to calculate the missed logs as well as effectively separated the litho-fluid facies in the heterogeneous sands of the Mehar gas field.

6 Conclusion

A successful study has been carried out to highlight the litho-fluid classification and enhanced reservoir depiction in the Mehar gas field using petrophysical analysis and rock physics modelling. The reservoirs selected for this work were sandstone of Lower Ranikot and Pab formations. Three wells (Mehar-01, 02, and 03) data have been used to perform petrophysical interpretation and rock physics modelling. The integrated and iterative log data conditioning, seismic petrophysics interpretation, rock physics template, and seismic well ties workflow enabled the generation of a rock physics model that has been successfully used to correct poor-quality data and synthesize missing elastic logs, especially P-sonic and S-sonic in the utilized wells. Cross-plot analysis of petro-elastic attributes fairly discriminated the facies into gas sand, wet sand, shale, and limestone. The modelled logs show improved data quality and consistency between the wells of the Mehar gas field.

Acknowledgments: All the authors would like to thank the Directorate General of Petroleum Concessions (DGPC), Pakistan, for being a data source for this work. The authors would also like to thank the Department of Earth Sciences, Quaid-i-Azam University (QAU), Islamabad, Pakistan, Department of Earth and Environmental Sciences, Bahria University, Islamabad, Pakistan, Compagnie Générale de Géophysique (CGG), and LMK Resources (LMKR) Pakistan for providing the necessary software and laboratory support to complete this work.

Authors contributions: Urooj Shakir did the manuscript writing along with the technical work. Aamir Ali supervised the research and provided guidance and valuable assistance in technical writing. Muyyassar Hussain

supported the technical workflow execution of the software. Muhammad Raiees Amjad helped in literature review and petrophysical analysis.

Conflict of interest: Authors state no conflict of interest.

References

[1] Li G, Li G, Wang Y, Qi S, Yang J. A rock physics model for estimating elastic properties of upper Ordovician-lower Silurian mudrocks in the Sichuan Basin, China. Eng Geol. 2020;266:105460.
[2] Ghosh D, Babasafari A, Ratnam T, Sambo C, editors. New workflow in reservoir modelling-incorporating high resolution seismic and rock physics; 2018. Offshore Technology Conference Offshore Technology Conference Asia.
[3] Bredesen K, Jensen EH, Johansen TA, Avseth P. Quantitative seismic interpretation using inverse rock physics modelling. Pet Geosci. 2015;21(4):271–84.
[4] Babasafari AA, Ghosh DP, Salim AM, Kordi M. Integrating petroelastic modeling, stochastic seismic inversion, and Bayesian probability classification to reduce uncertainty of hydrocarbon prediction: Example from Malay Basin. Interpretation. 2020;8(3):SM65–82.
[5] Dvorkin J, Gutierrez MA, Grana D. Seismic reflections of rock properties. England, UK: Cambridge University Press; 2014.
[6] Saberi MR. A closer look at rock physics models and their assisted interpretation in seismic exploration. Iran J Geophysics. 2017;10(5):71–84.
[7] Dou Q, Sun Y, Sullivan C. Rock-physics-based carbonate pore type characterization and reservoir permeability heterogeneity evaluation, Upper San Andres reservoir, Permian Basin, west Texas. J Appl Geophysics. 2011;74(1):8–18.
[8] Azeem T, Chun WY, Khalid P, Ehsan MI, Rehman F, Naseem AA. Sweetness analysis of lower Goru sandstone intervals of the Cretaceous age, Sawan gas field, Pakistan. Epis J Int Geosci. 2018;41:235–47.
[9] Azeem T, Chun WY, Khalid P, Qing LX, Ehsan MI, Munawar MJ, et al. An integrated petrophysical and rock physics analysis to improve reservoir characterization of Cretaceous sand intervals in middle Indus Basin, Pakistan. J Geophysics Eng. 2017;14(2):212–25.
[10] Babasafari A, Ghosh D, Salim AM, Alashloo SM. Rock physics modeling assisted reservoir properties prediction: case study Malay Basin. Int J Eng Technol. 2018;7(3):24–8.
[11] Jensen EH, Johansen TA, Avseth P, Bredesen K. Quantitative interpretation using inverse rock-physics modeling on AVO data. Lead Edge. 2016;35(8):677–83.
[12] Sohail GM, Hawkes CD. An evaluation of empirical and rock physics models to estimate shear wave velocity in a potential shale gas reservoir using wireline logs. J Pet Sci Eng. 2020;185:106666.
[13] Avseth P, Skjei N. Rock physics modeling of static and dynamic reservoir properties – a heuristic approach for cemented sandstone reservoirs. Lead Edge. 2011;30(1):90–6.
[14] Karimpouli S, Khoshlesan S, Saenger EH, Koochi HH. Application of alternative digital rock physics methods in a real case study: a challenge between clean and cemented samples. Geophys Prospecting. 2018;66(4):767–83.
[15] Sayers CM, den Boer LD. Rock physics-based relations for density and S-velocity versus P-velocity in deepwater subsalt Gulf of Mexico shales. Lead Edge. 2011;30(12):1376–81.
[16] Dou Q, Sun Y, Sullivan C. Rock-physics-based heterogeneity characterization of a carbonate reservoir in the Permian Basin. SEG Technical Program Expanded Abstracts 2009: Society of Exploration Geophysicists; 2009. p. 1945–9.
[17] Ajisafe Y, Ako B. 3-D seismic attributes for reservoir characterization of "Y" field Niger Delta, Nigeria. IOSR J Appl Geol Geophysics. 2013;1(2):23–31.
[18] Magoba M, Opuwari M. Petrophysical interpretation and fluid substitution modelling of the upper shallow marine sandstone reservoirs in the Bredasdorp Basin, offshore South Africa. J Pet Exploration Prod Technol. 2020;10(2):783–803.
[19] Grana D. Bayesian linearized rock-physics inversion. Geophysics. 2016;81(6):D625–41.
[20] Babasafari AA, Khoshdel H, editors. Mapping reservoir fluid using AVO inversion. In: 6th EAGE Saint Petersburg International Conference and Exhibition. Houten, The Netherlands: European Association of Geoscientists & Engineers; 2014.
[21] Ahmed N, Khalid P, Shafi HMB, Connolly P. DHI evaluation by combining rock physics simulation and statistical techniques for fluid identification of Cambrian-to-Cretaceous clastic reservoirs in Pakistan. Acta Geophysica. 2017;65(5):991–1007.
[22] Xu S, Payne MA. Modeling elastic properties in carbonate rocks. Lead Edge. 2009;28(1):66–74.
[23] Dvorkin J. Seismic reflections of rock properties. Hart's E & P. 2004;77(11):59–61.
[24] Liu Z, Sun SZ. The differential Kuster–Toksöz rock physics model for predicting S-wave velocity. J Geophysics Eng. 2015;12(5):839–48.
[25] Avseth P, Mukerji T, Mavko G, Dvorkin J. Rock-physics diagnostics of depositional texture, diagenetic alterations, and reservoir heterogeneity in high-porosity siliciclastic sediments and rocks – A review of selected models and suggested work flows. Geophysics. 2010;75(5):75A31–47.
[26] Waters KD, Kemper MA. Find the rocks and the fluids will follow – AVO as a tool for lithology classification. Interpretation. 2014;2(2):SC77–91.
[27] Greenberg M, Castagna J. Shear-wave velocity estimation in porous rocks: theoretical formulation, preliminary verification and applications1. Geophys Prospecting. 1992;40(2):195–209.
[28] Hashin Z, Shtrikman S. A variational approach to the elastic behavior of multiphase materials. J Mech Phys Solids. 1963;11(2):127–40.
[29] Wyllie MRJ, Gregory AR, Gardner LW. Elastic wave velocities in heterogeneous and porous media. Geophysics. 1956;21(1):41–70.
[30] Wyllie MRJ. The fundamentals of well log interpretation. Prentice Hall, New York: Academic Press; 1963.
[31] Avseth P, Bachrach R. Seismic properties of unconsolidated sands: Tangential stiffness, V_p/V_s ratios and diagenesis. SEG Technical Program Expanded Abstracts 2005: Society of Exploration Geophysicists; 2005. p. 1473–6.
[32] Babasafari AA, Bashir Y, Ghosh DP, Salim AMA, Janjuhah HT, Kazemeini SH, et al. A new approach to petroelastic modeling of carbonate rocks using an extended pore-space stiffness

method, with application to a carbonate reservoir in Central Luconia, Sarawak, Malaysia. Lead Edge. 2020;39(8):592a1–10.
[33] Rathore R, Hoo C, editors. Rock physics modeling in oil and gas field development: a methodology for reservoir characterization in low salinity pay. Seismic Driven Reservoir Characterization and Production Management. Houten, The Netherlands: European Association of Geoscientists & Engineers; 2015.
[34] Szeliga W, Bilham R, Schelling D, Kakar DM, Lodi S. Fold and thrust partitioning in a contracting fold belt: Insights from the 1931 Mach earthquake in Baluchistan. Tectonics. 2009;28(5):1–13.
[35] Arshad K, Imran M, Iqbal M, editors. Hydrocarbon prospectivity and risk analysis of an under-explored Western Kirthar fold belt of Pakistan. Offshore Mediterranean Conference and Exhibition; 2013. Offshore Mediterranean Conference.
[36] Fitzsimmons R, Buchanan J, Izatt C. The role of outcrop geology in predicting reservoir presence in the Cretaceous and Paleocene successions of the Sulaiman Range, Pakistan. AAPG Bull. 2005;89(2):231–54.
[37] Ahmad N, Fink P, Sturrock S, Mahmood T, Ibrahim M. Sequence stratigraphy as predictive tool in lower goru fairway, lower and middle Indus platform, Pakistan. PAPG, ATC. 2004;1:85–104.
[38] Wandrey CJ, Law B, Shah HA. Sembar Goru/Ghazij composite total petroleum system, Indus and Sulaiman-Kirthar geologic provinces. Pakistan and India: US Department of the Interior, US Geological Survey; 2004.
[39] Hinsch R, Asmar C, Hagedorn P, Nasim M, Rasheed MA, Stevens N, et al. Structural modelling in the kirthar fold belt of pakistan: from seismic to regional scale. AAPG/SEG, International Conference and Exhibition, London, UK; 2018.
[40] Zafar ZA, Shoaib K, Afsar F, Raja ZA, Tanveer A, Burley S, editors. A radical seismic interpretation re-think resolves the structural complexities of the Zamzama Field, Kirther Foredeep, Pakistan. PAPG. In: Islamabad, Pakistan: SPE Annual Technical Conference; December 2018.
[41] Ogilvie SR, Isakov E, Glover PW. Fluid flow through rough fractures in rocks. II: A new matching model for rough rock fractures. Earth Planet Sci Lett. 2006;241(3–4):454–65.
[42] Grana D, Pirrone M, Mukerji T. Quantitative log interpretation and uncertainty propagation of petrophysical properties and facies classification from rock-physics modeling and formation evaluation analysis. Geophysics. 2012;77(3):WA45–63.
[43] Akhter G, Ahmed Z, Ishaq A, Ali A. Integrated interpretation with Gassmann fluid substitution for optimum field development of Sanghar area, Pakistan: a case study. Arab J Geosci. 2015;8(9):7467–79.
[44] Shah MS, Khan MHR, Rahman A, Islam MR, Ahmed SI, Molla MI, et al. Petrophysical evaluation of well log data for reservoir characterization in Titas gas field, Bangladesh: a case study. J Nat Gas Sci Eng. 2021;95:104129.
[45] Wawrzyniak-Guz K. Rock physics modelling for determination of effective elastic properties of the lower Paleozoic shale formation, North Poland. Acta Geophys. 2019;67(6):1967–89.
[46] Ali A, Alves TM, Saad FA, Ullah M, Toqeer M, Hussain M. Resource potential of gas reservoirs in South Pakistan and adjacent Indian subcontinent revealed by post-stack inversion techniques. J Nat Gas Sci Eng. 2018;49:41–55.
[47] Rider MH. The geological interpretation of well logs. USA: Halsted Press; 1986.
[48] Reine C. Discovering a supermodel-A rock-Physics tutorial. CSEG Recorder. 2017;42(2):20–5.
[49] Mavko G, Mukerji T, Dvorkin J. The rock physics handbook. England, UK: Cambridge University Press; 2020.
[50] Batzle M, Wang Z. Seismic properties of pore fluids. Geophysics. 1992;57(11):1396–408.
[51] Ogbamikhumi A, Igbinigie NS. Rock physics attribute analysis for hydrocarbon prospectivity in the Eva field onshore Niger Delta Basin. J Pet Exploration Prod Technol. 2020;10(8):3127–38.
[52] Abbey CP, Okpogo EU, Atueyi IO. Application of rock physics parameters for lithology and fluid prediction of 'TN'field of Niger Delta basin, Nigeria. Egypt J Pet. 2018;27(4):853–66.
[53] Omudu L, Ebeniro J. Cross-plotting of rock properties for fluid discrimination using well data in offshore Niger Delta. Nigerian J Phys. 2005;17(1):16–20.
[54] Da-Xing W. A study on the rock physics model of gas reservoir in tight sandstone. Chin J Geophysics. 2017;60(1):64–83.
[55] Yasin Q, Sohail GM, Khalid P, Baklouti S, Du Q. Application of machine learning tool to predict the porosity of clastic depositional system, Indus Basin, Pakistan. J Pet Sci Eng. 2021;197:107975.
[56] Fitch P, Davies S, Lovell M, Pritchard T. Reservoir quality and reservoir heterogeneity: petrophysical application of the Lorenz coefficient. Petrophysics. 2013;54(5):465–74.